UDK 621.791.725:669.715
Original scientific article/Izvirni znanstveni članek

ISSN 1580-2949
Mater. Tehnol.

MICROSTRUCTURE CHARACTERISATION OF THE LASER-HYBRID-WELDED ALUMINIUM ALLOY EN AW-5454-D

KARAKTERIZACIJA MIKROSTRUKTURE LASERSKO HIBRIDNO ZAVARJENE AL-ZLITINE EN AW-5454-D

Matjaž Balant[1*], Črtomir Donik[2], Tomaž Vuherer[1], Rebeka Rudolf[1,3,4]

[1]University of Maribor, Faculty of Mechanical Engineering, Maribor, Smetanova ul. 17, Slovenia
[2]Institute of Metals and Technology, Lepi pot 11, Ljubljana, Slovenia
[3]Zlatarna Celje d.o.o., Kersnikova ul. 19, Celje, Slovenia
[4]Pomurje Science and Innovation Centre, 9000 Murska Sobota, Slovenia

Prejem rokopisa – received: 2025-01-20; sprejem za objavo – accepted for publication: 2025-03-20

doi:10.17222/mit.2024.1384

Microstructural characterisation was performed on EN AW-5454-D Al-alloy weld samples made with a laser-hybrid-welding process in a horizontal position. For this purpose, two pre-bent Al-sheets were used, with different thicknesses of 3.5 and 4 mm. The microstructural characterisation included scanning electron microscopy with microchemical analysis and electron-backscatter diffraction, as well as optical microscopy. The characterisation revealed that the microstructure consists of a primary α-aluminium phase and a minor Al_6Mn phase. A fine-grained microstructure was identified in the weld metal. Hardness measurements of HV 0.5 were performed in the weld joint, where the results revealed that the hardness was reduced in the weld metal and the heat-affected zone in comparison with the base metal. A theoretical calculation of the chemical composition in selected areas of the weld was performed, which was compared with the results of EDX microchemical analysis obtained for each element. The comparison showed relatively good agreement.

Keywords: Al-alloy, microstructure, laser-hybrid welding, characterisation

Izvedena je bila mikrostrukturna karakterizacija vzorca zvara Al-zlitine EN AW-5454-D, ki je bil izdelan z lasersko hibridnim postopkom varjenja v vodoravnem položaju. Za ta namen sta bili uporabljeni dve predhodno upognjeni Al-pločevini z različnima debelinama 3.5 in 4 mm. Mikrostrukturna karakterizacija je vključevala vrstično elektronsko mikroskopijo z mikrokemično analizo in difrakcijo povratnega sipanja elektronov. Karakterizacija je odkrila, da se mikrostruktura sestoji iz primarne faze α-aluminija, in manjšinske faze Al_6Mn. V varu je bila identificirana drobnozrnata mikrostruktura. Na zvarnem spoju so bile opravljene meritve trdote HV 0.5, ki so odkrile, da je trdota v varu in toplotno vplivanem področju manjša v primerjavi z osnovnim materialom. Izveden je bil teoretičen izračun kemijske sestave v izbranih področjih zvara, ki je bil primerjan z dobljenimi rezultati EDX mikrokemične analize za posamezen element. Primerjava je pokazala relativno dobro ujemanje.

Ključne besede: Al-zlitina, mikrostruktura, lasersko-hibridno varjenje, karakterizacija

1 INTRODUCTION

Due to the well-known properties of the Al-alloy EN AW-5454-D, such as good formability[1] and weldability,[2] a favourable density-loading ratio[3,4] and excellent mechanical properties,[5–7] this alloy is very suitable for use in the automotive industry in terms of weight reduction and environmental footprint[8,9] due to the lower consumption of energy sources for vehicle propulsion. [10]

Laser hybrid welding compensates for the individual disadvantages of the laser and arc welding.[11] In the field of Al-alloy welding, practices and optimal technological parameters are not known. The determination of the optimal technological parameters to produce the individual structural elements and for individual Al-alloys is still in the experimental phase. When choosing the optimal parameters, laser hybrid welding offers many advantages[12] over conventional welding processes, as it is much faster and more productive than conventional arc welding,[13] it ensures less heat input[14–16] to the weld joint, and, as a result, a lower energy consumption, it enables the bridging of larger clearances between individual parts,[17] enables a better appearance of the welds and reduces defects in the welds.[18,19] Due to the lower heat input there are smaller changes in the microstructure in the heat-affected zone (HAZ),[20–22] residual stresses[23] and related deformations due to the large expansions and contractions of Al-alloys.[24,25]

During laser hybrid welding an absorption of the laser beam occurs, depending on the temperature of the surface of the welds. At the beginning of the welding it is necessary to overcome the initial reflection, especially with Al-alloy welds. When the evaporation temperature is reached an evaporation cavity – a keyhole – is formed, which causes almost the entire energy of the beam to be absorbed in the weld.[17]

In laser hybrid welding, due to local high heat input and melting of the alloy and dilution rate in the weld

*Corresponding author's e-mail:
matjaz.balant@student.um.si (Matjaž Balant)

Table 1: Chemical composition of the Al-alloy EN AW-5454-D (in *w*/%)

Thickness [mm]	Element	Si	Fe	Cu	Mn	Mg	Cr	Zn	Ti	Al
3.5		0.16	0.31	0.06	0.79	2.86	0.07	0.03	0.02	95.70
4.0		0.18	0.32	0.05	0.76	2.85	0.05	0.04	0.02	95.73

zone, some of the minority Al_6Mn phase dissolved in the α-aluminium phase,[1,5,7,18,24] which was studied in this research.

The investigated Al-alloy of the base material belongs to the 5XXX group, which is characterised by being hardened by kneading.[26–34] With welding and the introduction of heat the material softens in the area of the weld joint, and acquires the values of the undeformed base material.[1,4,21,26] In order to preserve the mechanical properties of the base material, it is necessary to ensure that the heat input and the resulting thermally affected area are as small as possible,[15,35] but sufficient to ensure the subsequent load-bearing capacity of the weld joint.

The aim of this study of a laser-hybrid welded joint made of the Al-alloy EN AW-5454-D was to investigate the microstructural changes in the weld joint, and to determine their influence on the mechanical properties. With pre-selected technological welding parameters, the focus was to minimise the formation of defects in the weld,[36–39] which, later, have a significant influence on the construction integrity. Various analytical techniques were used for the characterisation.

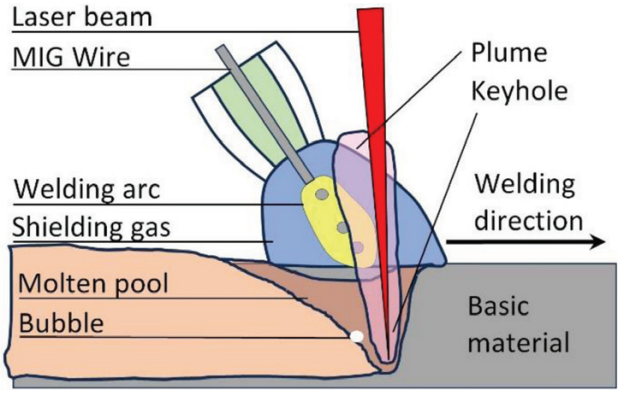

Figure 1: Schematic of elements during laser hybrid welding

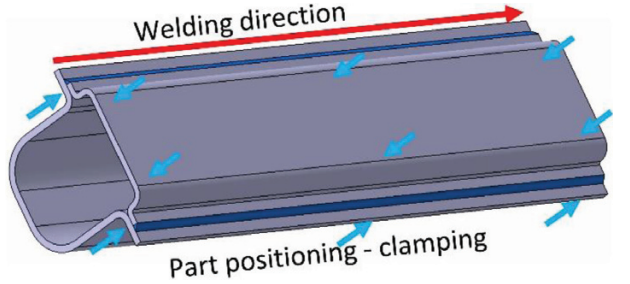

Figure 2: Schematic of weldment clamping during laser hybrid welding

2 MATERIALS AND METHODS

2.1 Base material

Base materials supplied by Speira GmbH (Grevenbroich, Germany) were used for the investigations. The test samples were made from cold-rolled sheet metal of two thicknesses (3.5 mm and 4 mm). The plates rolled in the longitudinal direction were cut and formed into the desired shape of the parts. The chemical composition of the supplied Al-alloy EN AW-5454-D used for the tests and analyses is listed in **Table 1**.

2.2 Filler material

For welding, we used a filler material supplied by the manufacturer Safra Spa (Travagliato, Italy). A massive welding wire was used, i.e., Safra Al Mg2.7Mn (S Al5554 – EN ISO 18273); wire diameter Ø 1.6 mm.

The chemical composition of the supplied welding wire used for the tests and analyses is listed in **Table 2**.

Table 2: Chemical composition of the welding wire Al5554 (in *w*/%)

Cr	Cu	Fe	Mg	Mn	Si	Ti	Zn	Al
0.079	0.0019	0.148	2.83	0.609	0.057	0.088	0.0018	Rest

2.3 Sample preparation

2.3.1 Welding

Figure 1 shows the individual elements during the laser hybrid welding. The Al-sheet samples were welded robotically in a welding cell for safety reasons. Due to the robotic welding and complex shape, it was necessary to position and clamp the weldments in the welding fixture accurately, are shown schematically in **Figure 2**.

A laser welding source IPG YLS-4000 (IPG Laser GmbH, Allershausen, Germany), a welding source for MIG welding process: Fronius TransPuls Synergic 5000 R (Fronius, Austria) and a laser hybrid welding head Fronius (Fronius, Wels, Austria) were used for the laser hybrid welding. The technological parameters for laser hybrid welding of the lap weld are listed in **Table 3**.

Table 3: Technological parameters for laser hybrid welding

Welding parameter	Value
Welding position	PA-Flat position
Shielding gas	100 % Ar
Welding speed	270 cm/min
Wire feed speed	6.07 m/min
Welding current	220 A
Voltage	21 V
Laser power	2000 W
Type of welding current and polarity	AC-Pulse

2.3.2 Metallographic sample preparation

The weld samples were cut with a band saw from the middle of the formed weld. A range of standardised analytical techniques was employed to gain a clear and detailed understanding of the microstructure of the metallographic samples. These included mounting the samples in conductive Bakelite resin, grinding and polishing them carefully, and finishing them with an oxide polishing suspension (OPS) from Schmitz-Metallographie for 10 min.

2.4 Characterisation

2.4.1 Microstructural analysis and EDS analysis

A Zeiss CrossBeam 550 FIBSEM field-emission scanning electron microscope (Carl Zeiss, Jena, Germany) was used, equipped with an EDAX Hikari Super electron-backscatter diffraction (EBSD) camera and EDAX Octane Elite energy-dispersive spectroscopy (EDS) detector with APEX software for detailed analyses. This allowed for various analyses, including secondary-electron imaging, EDS and EBSD. To achieve the most suitable results a range of parameters were employed, including a 15-kV accelerating voltage and 2.0–5.0-nA probe current for the SE images.

2.4.2 Microchemical analysis in the field of welding

The welded areas marked in **Figure 3** were examined and analysed by microchemical EDX analysis on an FEI Sirion 400 NC microscope, which is equipped for microchemical analysis with an energy dispersion spectrometer, EDS Oxford INCA 350. The samples were analysed from secondary- and backscattered-electron images at magnifications of 500× to 10,000×, with an acceleration voltage of 20 kV and an electron beam spot size of 3.0–4.0. The EDX analysis was conducted in the range 0–20 keV, for elemental determination of the analysed sites, with normalised results. EDX chemical analyses were performed on three cross-sections of the weld, and the average of the individual chemical elements was calculated based on the selected places.

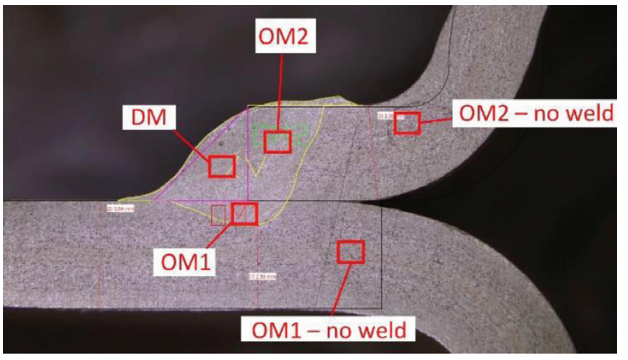

Figure 3: Selected places where EDX analyses were performed inside of the weld area: OM1 = melted base material 1 and filler material, OM2 = melted base material 2 and filler material, DM = melted filler material and melted base materials 1 and 2; outside of weld area: OM1 – no weld = base material 1, OM2 – no weld = base material 2

2.4.3 EBSD analysis

The EBSD analysis was performed on a ZEISS FIB-SEM CrossBeam 550 device (Carl Zeiss AG, Oberkochen, Germany) with an integrated EDAX Hikari super EBSD camera (Ametek Inc., Bervyn, PA, USA). During the EBSD analysis, an inclination angle of 70° was used, with an acceleration voltage of 15 kV and a probe current of 10 nA. The data were analysed using the EDAX OIM 9 software package.

2.4.4 Hardness measurements

To obtain a better insight into the state of the weld joint, the HAZ area and the surroundings of the weld joint, we performed an automated measurement of microhardness HV0.5 over the entire area with a selected measuring grid of 0.5 mm. The automated HV0.5 hardness measurements were performed on a DuraScan 50 G5 (EMCO-TEST Prüfmaschinen GmbH, Kuchl, Austria) in accordance with the ISO 6507 Standard. The hardness of the samples was examined on the previously metallographically prepared samples.[40] The measurement load of 0.5 kg was selected for the given sample dimensions. The data were analysed using the software package.

2.4.5 Calculation of the theoretical dilution rate

On the three metallographically prepared weld-joint samples, contours and measurements of the weld surfaces were performed using the DraftSight 2022 software (Dassault Systèmes, Paris, France). These areas were converted into shares of the total area using equations 1 and 2:

$$A_{ZV} = A_{OM1} + A_{OM2} + A_{DM} \quad (1)$$

$$S_{OM1} = \frac{A_{OM1}}{A_{ZV}};\ S_{OM2} = \frac{A_{OM2}}{A_{ZV}};\ S_{DM} = \frac{A_{DM}}{A_{ZV}} \quad (2)$$

where A_{ZV} is the total surface of the weld, A_{OM1} is the melted surface of base material 1, A_{OM2} is the melted surface of base material 2, A_{DM} is the surface of the filler material, S_{OM1} is the proportion of the surface of base material 1, S_{OM2} is the proportion of the surface of base material 2, S_{DM} is the proportion of the surface of the filler material. The theoretical dilution rate of each of the melted surfaces of the base material were mixed with filler material according to the key written in **Table 4** and statistical evaluations of the data were performed using the MS Excel software.

Table 4: Theoretical dilution rates

Weld area	Theoretical dilution rates
A_{OM1}	50 % OM1 50 % DM
A_{OM2}	50 % OM2 50 % DM
A_{DM}	% of OM1 surface % of OM2 surface % of DM surface

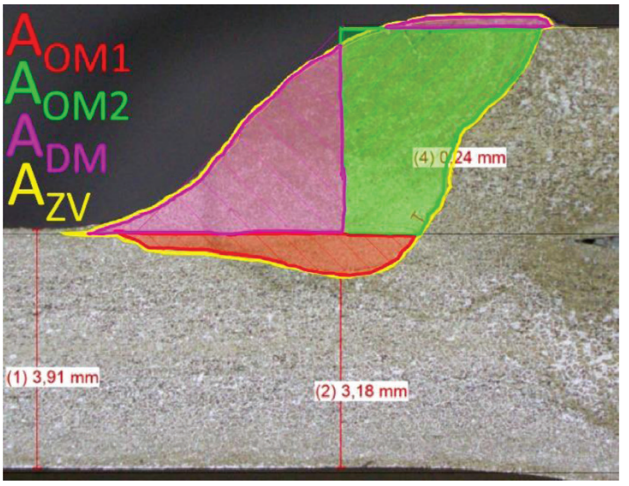

Figure 4: Weld areas: A_{OM1} – melted surface of base material 1; A_{OM2} – melted surface of base material 2; A_{DM} – melted surface of the filler material; A_{ZV} –total surface of the weld

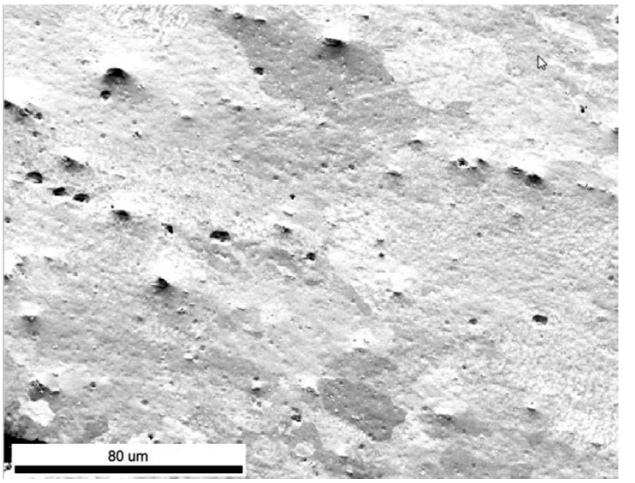

Figure 5: SEM microstructure of the weld-joint area in the root region

Figure 4 shows the individual weld areas that were considered in the calculations.

3 RESULTS

3.1 Microstructure

Figure 5 shows an SEM micrograph of the weld metal. The examination revealed that the microstructure was relatively homogeneous with an unevenly distributed minority phase Al_6Mn that appeared as black areas. In some places the concentration of the minority phase Al_6Mn was higher, and the estimated size of this phase was 3 µm. In some areas, α-aluminium-phase grains can be seen, the size of which was estimated to be between 40 µm and 100 µm in the longitudinal direction.

3.2 Chemical composition in the field of welding: EDS analysis

A spot EDS analysis was performed at 21 places in each weld metal. The content was determined for the elements Al, Si, Fe, Cu, Mn, Mg, Cr, Zn and Ti. The calculated averages of the content of chemical elements according to the individual areas of the welds are given in **Table 5**.

3.3 EBSD analysis

Figure 6a shows the weld-joint area. The selected macro-region (red rectangle) shows the area where the EBSD analysis was performed. **Figure 6b** presents the EBSD analysis, where well-detected grains and their orientations are visible. The boundary separating the coarse-grained (HAZ) and fine-grained (weld metal) areas is marked with a black line. The estimated size of the larger grains in the HAZ was, on average, 15 µm, and smaller ones in the weld metal around 4 µm. The grains in the HAZ were oriented and had a characteristic texture, while the grains in the weld metal area had a globular characteristic. The EBSD analysis revealed that the majority α-aluminium phase surface fraction was 99 % in the analysed area, and that the minority phase Al_6Mn had a fraction of about 1 %, as shown in **Figure 6c**. The estimated average size of the minority phase Al_6Mn was around 3 µm.

Table 5: Results of the microchemical EDX analysis in individual areas of the weld (in *w*/%)

Weld area	Al	Si	Fe	Cu	Mn	Mg	Cr	Zn	Ti
A_{OM1}	95.50	0.37	0.28	0.06	0.79	2.84	0.09	0.04	0.05
min	95.32	0.25	0.21	0	0.72	2.70	0.01	0	0.01
max	95.65	0.46	0.39	0.11	0.85	2.95	0.11	0.08	0.10
SD	0.12	0.07	0.06	0.04	0.05	0.09	0.04	0.03	0.03
A_{OM2}	95.38	0.36	0.26	0.06	0.86	2.97	0.04	0.02	0.06
min	95.14	0.22	0.18	0	0.80	2.85	0.03	0	0
max	95.62	0.45	0.37	0.14	0.95	3.14	0.07	0.04	0.17
SD	0.16	0.08	0.06	0.05	0.05	0.10	0.01	0.02	0.06
A_{DM}	95.36	0.57	0.28	0.01	0.79	2.81	0.09	0.05	0.04
min	95.15	0.48	0.23	0	0.72	2.63	0.05	0	0
max	95.68	0.68	0.33	0.04	0.84	3.01	0.16	0.13	0.08
SD	0.17	0.08	0.04	0.02	0.05	0.11	0.05	0.04	0.03

3.4 Hardness HV0.5

Figure 7a shows a macro-section of the weld joint, where a mesh of the generated HV0.5 impressions is visible. The grid was made in such a way that the distance between the impressions equalled 0.5 mm. In this way, the entire surface was included in the hardness measurements and thus evenly on the selected weld joint. A graphical representation of the measurement results with a value between 60 and 100 HV0.5 is shown in **Figure 7b**. **Figure 7** shows the HAZ within the red lines, where the fusion line is denoted by a line-dot-dot-line, and the dashed line represents the boundary between the unaffected base material and the HAZ.

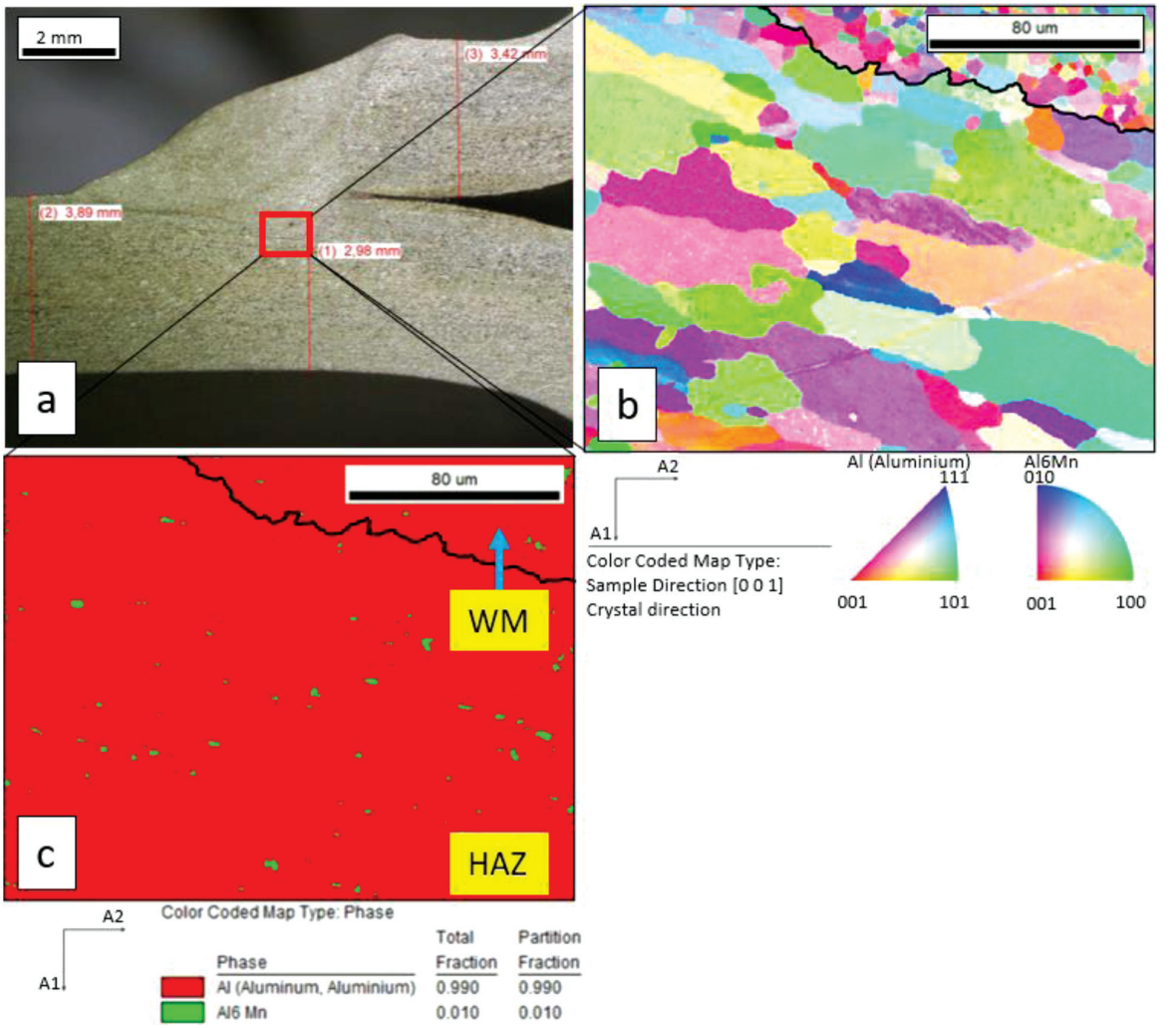

Figure 6: Weld-joint area in the root region: a) Macro-section of the weld joint; b) EBSD analysis of the microstructure; c) Phase structure: α-aluminium phase (red) and minority phase Al_6Mn (green)

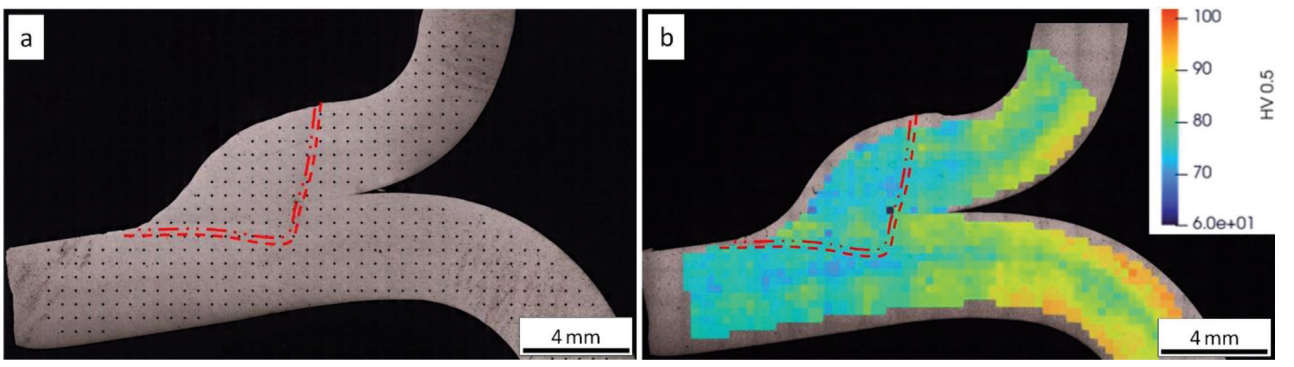

Figure 7: a) Macro-section with a network of impressions; b) Complementary presentation of the HV0.5 results

Table 6 contains the statistical data of the HV0.5 measurements performed in individual areas. In the base material, the average value of HV0.5 was 81.1, in the HAZ area 77.9, and in the weld joint 75.5. The largest dispersion of measurements was in the base material, and the smallest in the HAZ area.

Table 6: Results of the HV0.5 hardness measurements

Weld area	Base material	HAZ	Weld
Average	81.1	77.9	75.5
min	70.5	68.5	56
max	96.8	84	85.2
SD	5.7	3.2	3.3

3.5 Theoretical calculations of dilution rate

Calculations of the dilution rate were performed for 6 samples, according to the predicted ratios from Table 4 and depending on the surface of the weld joint. The calculated average contents of individual elements are shown in **Table 7**.

The deviations between the averages of the results of the EDS microchemical analysis and the calculated averages of the theoretical calculations were calculated, which is shown in **Table 8** as the deviation.

The largest deviations were detected for Al and Si in the weld area, i.e., 0.53 *w*/% for Al and 0.44 *w*/% for Si. The deviations for the other microalloying elements were less than 0.1 *w*/%.

4 DISCUSSION

The microstructure of the base material EN AW-5454-D was analysed in detail in the article of authors Balant, et al.[41,42] The used EBSD analysis revealed the presence of a minority phase Al_6Mn with a surface proportion between 1.2 % and 2.6 % in the α-aluminium phase. A similar EBSD analysis was performed in the root region of the weld joint. The results of this analysis in the HAZ showed that the minority phase Al_6Mn was reduced to approximately 1 % due to heat input during welding. Consequently, this minority phase Al_6Mn was partly dissolved in the α-aluminium phase due to the temperature increase. This resulted in a decrease of the surface proportion of the minority phase Al_6Mn. The minority Al_6Mn phase was relatively uniformly distributed in the weld joint, with an estimated average size of 3 µm. In the weld metal, where melting occurred during welding, the temperature was even higher. This resulted in almost complete dissolving of the minority phase Al_6Mn in the α-aluminium phase. Due to melting in the weld metal, the material in the weld pool recrystallised again. This resulted in a smaller grain size (from 0.5 µm to approx. 10 µm). In these grains, the minority phase Al_6Mn was small in the surface proportion and hard to detect.

The reviewed literature[1,20,43] indicates that the minority phase of $Al_6(Mn, Fe)$ is also present in the Al-alloy EN AW-5454-D. At this stage, the elements Mn and Fe can occur in different relationships to each other, depending on the state of the Al-alloy. The EBSD analysis revealed a minority phase in the analysed area, written as Al_6Mn, which means that, in this region, this analysis did not detect Fe. The EDS analysis revealed a chemical composition that included not only Mn, but also Fe in different ratios. The EDS analysis is volumetric, because, in addition to the analysed area, it also captures a certain volume of the alloy below the analysis area.[44–47] Based on the above observations, we can conclude that both chemical elements occurred in the minority phase, which can be written as $Al_6(Mn, Fe)$.

Table 7: Theoretical calculation – average values for individual elements (in *w*/%)

Weld area	Al	Si	Fe	Cu	Mn	Mg	Cr	Zn	Ti
A_{OM1}	95.96	0.12	0.23	0.03	0.68	2.84	0.06	0.02	0.05
min	95.96	0.12	0.23	0.03	0.68	2.84	0.06	0.02	0.05
max	95.96	0.12	0.23	0.03	0.68	2.84	0.06	0.02	0.05
SD	0	0	0	0	0	0	0	0	0
A_{OM2}	95.72	0.17	0.32	0.06	0.78	2.86	0.06	0.04	0.02
min	95.72	0.17	0.32	0.06	0.78	2.86	0.06	0.04	0.02
max	95.72	0.17	0.32	0.06	0.78	2.86	0.06	0.04	0.02
SD	0	0	0	0	0	0	0	0	0
A_{DM}	95.89	0.12	0.25	0.04	0.72	2.85	0.07	0.02	0.05
min	95.87	0.12	0.24	0.03	0.71	2.85	0.07	0.02	0.04
max	95.91	0.13	0.26	0.04	0.72	2.85	0.07	0.02	0.05
SD	0.012	0.003	0.004	0.001	0.005	0.001	0	0.001	0.002

Table 8: Deviation of averages of the theoretical calculations from measured EDS analyses in individual areas of the weld (in *w*/%)

Weld area	Al	Si	Fe	Cu	Mn	Mg	Cr	Zn	Ti
A_{OM1}	0.46	0.25	0.04	0.03	0.10	0	0.02	0.01	0.01
A_{OM2}	0.34	0.19	0.06	0	0.09	0.12	0.02	0.02	0.04
A_{DM}	0.53	0.44	0.03	0.03	0.07	0.04	0.02	0.03	0

The average measured microhardness in the base material was 81.1 HV0.5, in the heat-affected area 77.9 HV0.5, and in the weld 75.5 HV0.5. The literature data also indicated that the hardness in individual areas of the material depends on previous mechanical processes[26,48,49] and from heat input during welding.[5,7] The above-mentioned arguments are the reason for the reduction of the number and the size of the obstacles present in the grains. Dislocations are easily movable within grains, which resulted in a hardness reduction in the weld metal and partially in the HAZ.[50]

The convenient hardened microstructure obtained by rolling,[51,26–28,30,33] gave favourable mechanical properties. During the welding process this microstructure changed due to the heat input, which affected the reduction of some mechanical properties, such as hardness. During rolling, the microstructure is strengthened, as most of the dislocations stop on the obstacles, which affects the increase of some mechanical properties (strength, hardness).[52–55] The study with the microstructural analysis revealed that obstacles which block the travel of dislocations are reduced significantly, resulting in less hardness, as the dislocations can become movable.

A review of the results of the EDS analysis and theoretical calculations of the placement of the base and filler material showed that there was a small deviation between the two methods for the chemical elements Al and Si, but for the other microalloying elements the deviations were less than 0.1%. This indicates a good agreement between the two methods. The theoretical model for calculating the proportions of individual chemical elements in the areas of the weld metal has been established relatively well. By comparing the chemical compositions of the base materials, filler material, calculated proportions of the chemical elements and EDS analysis, we can conclude that, depending on the type of base material, an appropriate filler material was selected, the selection of which was also recommended by the literature.[56–58] Based on the performed calculations, we can conclude that the predicted proportions of the dilution rates were determined relatively well, since, in general, there were no large deviations, and that EDS microchemical analysis can be used for such comparative analyses.

In addition, due to the clamping of the samples, which ensures the positioning of the parts during welding, residual stresses are introduced into the weld joint,[35,47,59,60–63] which cause deformations and, in extreme cases, a crack.[65] Since many residual stresses are concentrated in the root of the weld and the mechanical properties of the material deteriorate due to welding, it can be expected that, in the event of a change in conditions during laser hybrid welding, crack initiation might occur right in the root of the weld. Due to the above, it will be necessary to define the welding parameters in the future, where there will be no possibility of defects in the weld joint EN AW-5454-D Al-alloy during laser hybrid welding.

5 CONCLUSIONS

The investigation of the weld joint in the Al alloy EN AW-5454-D led to the following conclusions:

- In the weld metal, the grain size was reduced from 9 μm in the base material to approximately 4 μm in the weld metal, caused by heat input and melting during welding.
- The surface portion of the minority phase Al_6Mn was reduced from 1.2–2.6 % in the base material to 1 % in the HAZ due to dissolving during welding. In the weld metal the minority phase Al_6Mn was almost completely dissolved. Only a small surface portion remained.
- The comparison of the theoretical calculation of the dilution rates with the EDS analysis showed a good agreement.
- The average measured microhardness in the base material was 81.1 HV0.5, in the HAZ 77.9 HV0.5, and in the weld metal 75.5 HV0.5.

Abbreviations:

A_{DM}	Surface of the filler material
A_{OM1}	Melted surface of base material 1
A_{OM2}	Melted surface of base material 2
A_{ZV}	The total surface of the weld metal
DM	Filler material
EBSD	Electron Back-Scattered Diffraction
EDX	Energy-Dispersive X-Ray spectroscopy
HAZ	Heat-Affected Zone
OM1	Base material 1
OM2	Base material 2
S_{DM}	Proportion of the surface of filler material
S_{OM1}	Proportion of the surface of base material 1
S_{OM2}	Proportion of the surface of base material 2
SEM	Scanning Electron Microscope
WM	Weld material

6 REFERENCES

[1] A. Salej Lah, M. Vončina, I. Paulin, J. Medved, P. Fajfar, D. Volšak, The influence of chemical composition and heat treatment on the mechanical properties and workability of the aluminium alloy EN AW 5454, Mater. Tehnol., 55 (**2021**), doi:10.17222/mit.2021.155

[2] L. M. Volpone, S. Mueller, Joints in light alloys today: the boundaries of possibility, Weld. Int., 22 (**2008**) 9, 597–609, doi:10.1080/09507110802411518

[3] K. Sheng, L. Lu, Y. Xiang, M. Ma, Z. Wu, Crack behavior in Mg/Al alloy thin sheet during hot compound extrusion, J. Magnes. Alloy., 7 (**2019**)4, 717–724, doi:10.1016/j.jma.2019.09.006

[4] A. V Mikhaylovskaya, V. K. Portnoy, A. G. Mochugovskiy, M. Y. Zadorozhnyy, N. Y. Tabachkova, I. S. Golovin, Effect of homogenisation treatment on precipitation, recrystallisation and properties of Al – 3% Mg – TM alloys (TM=Mn, Cr, Zr), Mater. Des., 109, (**2016**) 197–208, doi:10.1016/j.matdes.2016.07.010

[5] O. Engler, K. Kuhnke, J. Hasenclever, Development of intermetallic particles during solidification and homogenization of two AA 5xxx series Al-Mg alloys with different Mg contents, J. Alloys Compd., 728, (**2017**) 669–681, doi:10.1016/j.jallcom.2017.09.060

[6] J. Hirsch, Aluminium Alloys for Automotive Application, Mater. Sci. Forum – MATER SCI FORUM, 242 (**1997**) 33–50, doi:10.4028/www.scientific.net/MSF.242.33

[7] O. Engler, Z. Liu, K. Kuhnke, Impact of homogenization on particles in the Al–Mg–Mn alloy AA 5454 – Experiment and simulation, J. Alloys Compd., 560 (**2013**) 111–122, doi:10.1016/j.jallcom.2013.01.163

[8] J. Hirsch, T. Al-Samman, Superior light metals by texture engineering: Optimized aluminum and magnesium alloys for automotive applications, Acta Mater., 61 (**2013**) 3, 818–843, doi:10.1016/j.actamat.2012.10.044

[9] P. Krall, I. Weißensteiner, S. Pogatscher, Recycling aluminum alloys for the automotive industry: Breaking the source-sink paradigm, Resour. Conserv. Recycl., 202 (**2024**) 107370, doi:10.1016/j.resconrec.2023.107370

[10] I. García Gutiérrez, D. Elduque, C. Pina, R. Tobajas, C. Javierre, Influence of the Composition on the Environmental Impact of a Casting Magnesium Alloy, Sustainability, 12 (**2020**) 24, doi:10.3390/su122410494

[11] G. Casalino, U. Maso, A. Angelastro, S. L. Campanelli, Hybrid Laser Welding: A Review, DAAAM Int. Sci. B., (**2010**) 413–430

[12] C. Paul, J. Nicolae, Industrial applications for MSG – Laserhybrid welding process, Rev. Tehnol. Neconv., let. 15 (**2011**) 4

[13] H. Staufer, LaserHybrid welding for industrial applications, in Proceedings of SPIE – The International Society for Optical Engineering, 6346 (2**0**07) PART, doi:10.1117/12.738144

[14] ISO/TR 18491:2015 (E) Welding and allied processes – Guidelines for measurement of welding energies ISO Committee, Geneve

[15] DIN EN 1011-1:2009-07 (E) S Welding – Recommendations for welding of metallic materials – Part 1: General guidance for arc welding, DIN Deutsches Institut für Normung e. V., Berlin. Beuth Verlag GmbH, 10772 Berlin, Germany

[16] P. Leo, G. Renna, G. Casalino, A. G. Olabi, Effect of power distribution on the weld quality during hybrid laser welding of an Al–Mg alloy, Opt. Laser Technol., 73 (**2015**) 118–126, doi:10.1016/j.optlastec.2015.04.021

[17] B. J. Aalderink, B. Pathiraj, R. G. K. M. Aarts, Seam gap bridging of laser based processes for the welding of aluminium sheets for industrial applications, Int. J. Adv. Manuf. Technol., 48 (**2010**) 1-4, str. 143–154, doi:10.1007/s00170-009-2270-x

[18] S. Katayama, Fundamentals and Details of Laser Welding. Springer Singapore, (**2020**), doi:10.1007/978-981-15-7933-2

[19] Y. R. Ma, C. Cai, Z. J. Liu, J. Xie, C. Yang, Plasma Monitoring During Laser-MIG Hybrid Welding Process Based on LabVIEW, CHINESE J. LASERS-ZHONGGUO JIGUANG, 49 (**2022**) 2, doi:10.3788/CJL202249.0202014

[20] A. Kostrivas, J. C. Lippold, Fusion boundary microstructure evolution in aluminium alloys, Weld. World, let. 50 (**2006**) 11–12, 24–34, doi:10.1007/BF03263458

[21] P. Leo, S. D'Ostuni, G. Casalino, Hybrid welding of AA5754 annealed alloy: Role of post weld heat treatment on microstructure and mechanical properties, Mater. Des., 90 (**2016**), 777–786, doi:10.1016/j.matdes.2015.10.150

[22] V. Aleo, Effect of welding on the width of the heat -affected zone of aluminum alloys, ProQuest Dissertations Publishing, (2004).

[23] B. Çevik, B. Gülenç, The effect of welding speed on mechanical and microstructural properties of 5754 Al (AlMg3) alloy joined by laser welding, Mater. Res. Express, 5 (**2018**) 8, 86520, doi:10.1088/2053-1591/aad3b0

[24] M. Courbière, Welding Aluminum Alloys, in Metallurgy and Mechanics of Welding: Processes and Industrial Applications, Elsevier Scopus, (**2010**), 433–471

[25] B. Milkereit, O. Kessler, C. Schick, Chapter 18 – Recent Advances in Thermal Analysis and Calorimetry of Aluminum Alloys, in Recent Advances, Techniques and Applications, , S. Vyazovkin, N. Koga, C. B. T.-H. of T. A. and C. Schick, Ur. Elsevier Science B.V., 6 (**2018**) 735–779, doi:10.1016/B978-0-444-64062-8.00016-4

[26] A.-J. Mohammed, I. Maher, M. Nakai, M. A. H. Gepreel, Effects of cold rolling and heat treatment on the microstructure and hardness of pure aluminium, Mater. Today Proc., (**2023**), doi:10.1016/j.matpr.2023.09.138

[27] R. Uscinowicz, The effect of rolling direction on the creep process of Al–Cu bimetallic sheet, Mater. Des., 49, (**2013**), 693–700, doi:10.1016/j.matdes.2013.02.012

[28] A. Medjahed, H. Moula, A.Zegaoui, M. Derradji, A. Henniche, R. Wu, L. Hou, J. Zhang, M. Zhang, Influence of the rolling direction on the microstructure, mechanical, anisotropy and gamma rays shielding properties of an Al-Cu-Li-Mg-X alloy, Mater. Sci. Eng. A. Struct. Mater., let. 732 (**2018**) 129–137, doi:10.1016/j.msea.2018.06.074

[29] S. İriç, A. O. Ayhan, Dependence of Fracture Toughness on Rolling Direction in Aluminium 7075 Alloys, Acta Phys. Pol. A, 132 (**2017**) 3-II, 892–895, doi:10.12693/APhysPolA.132.892

[30] R. Sakin, Investigation of bending fatigue-life of aluminum sheets based on rolling direction, Alexandria Eng. J., 57 (**2018**) 1, 35–47, doi:10.1016/j.aej.2016.11.005

[31] H. Wang, Effect of rolling direction to texture evolution in an aluminium single crystal (011)[100]: a crystal plasticity FEM investigation, Mater. Res. express, 6 (**2019**) 12, doi:10.1088/2053-1591/ab17b4

[32] F. Lv, ,F. Yang, Q.Q. Duan, T.J. Luo, Y.S. Yang, S.X. Li, Z.F. Zhang, Tensile and low-cycle fatigue properties of Mg–2.8% Al–1.1% Zn–0.4% Mn alloy along the transverse and rolling directions, Scr. Mater., 61 (**2009**) 9, 887–890, doi:10.1016/j.scriptamat.2009.07.023

[33] I. Topic, H. W. Höppel, M. Göken, Influence of rolling direction on strength and ductility of aluminium and aluminium alloys produced by accumulative roll bonding, J. Mater. Sci., 43 (**2008**) 23–24, 7320–7325, doi:10.1007/s10853-008-2754-3

[34] A. Kazemi-Navaee, R. Jamaati, H. J. Aval, Asymmetric cold rolling of AA7075 alloy: The evolution of microstructure, crystallographic texture, and mechanical properties, Mater. Sci. Eng. A. Struct. Mater., 824 (**2021**), doi:10.1016/j.msea.2021.141801

[35] N. Nazemi, Identification of the mechanical properties in the heat-affected zone of aluminum welded structures, ProQuest Dissertations Publishing, (2015)

[36] EN ISO 13919-2:2021 (E) Electron and laser-beam welded joints – Requirements and recommendations on quality levels for imperfections – Part 2: Aluminium, magnesium and their alloys and pure copper, CEN-CENELEC Management Centre, Brussels

[37] Y. Takayama, Y. Kido, H. Kato, H. Watanabe, Microstructure and corrosion behavior in Al-Mg based alloys subjected to continuous cyclic bending and annealing, v Materials Science Forum, 654–656 (**2010**), 1002–1005, doi:10.4028/www.scientific.net/MSF.654-656.1002

[38] J. Kraner, P. Fajfar, H. Palkowski, M. Godec, I. Paulin, Asymmetric cold rolling of an aa 5xxx aluminium alloy, Mater. Tehnol., 54 (**2020**) 4, str. 575–582, doi:10.17222/mit.2020.097

[39] S. Yan, Z. Zhu, C. Ma, Q.-H. Qin, H. Chen, Y. N. Fu, Porosity formation and its effect on the properties of hybrid laser welded Al alloy joints, Int. J. Adv. Manuf. Technol., 104 (**2019**) 5, 2645–2656, doi:10.1007/s00170-019-04106-1

[40] E. Broitman, Indentation Hardness Measurements at Macro-, Micro-, and Nanoscale: A Critical Overview, Tribol. Lett., 65 (**2016**) 1, 23, doi:10.1007/s11249-016-0805-5

[41] M. Balant, R. Rudolf, Microstructure Characterization of Al-alloy AW 5454 Intended for Ecological Laser Hybrid Welding, Metall. Mater. Data, 2 (**2024**) 2, 59–64, doi::10.30544/MMD30

[42] M. Balant, R. Rudolf, Študija Al-zlitine AW 5454, ki je primerna za lasersko hibridno varjenje, IRT 3000 : inovacije, razvoj, tehnologije. – ISSN 1854-3669, 19 (**2024**) 148 (4), 67–69

[43] M. Osman, O. Engler, K. Karhausen, L. Löchte, A. J. McLaren, Effect of homogenisation conditions on recrystallisation in Al-Mg-Mn alloy AA 5454, Mater. Sci. Technol., 23 SE–1 (**2007**) 6, 688–698, doi:10.1179/174328407X179674

[44] S. Nasrazadani, S. Hassani, Chapter 2 – Modern analytical techniques in failure analysis of aerospace, chemical, and oil and gas industries, A. S. H. Makhlouf in M. B. T.-H. of M. F. A. with C. S. from the O. and G. I. Aliofkhazraei, Ur. Butterworth-Heinemann, (**2016**), 39–54, doi:10.1016/B978-0-08-100117-2.00010-8

[45] E. J. Payton, G. Nolze, The Backscatter Electron Signal as an Additional Tool for Phase Segmentation in Electron Backscatter Diffraction, Microsc. Microanal., 19 (**2013**) 4, 929–941, doi:10.1017/S1431927613000305

[46] Z. Hajizadeh, R. Taheri-Ledari, F. R. Asl, 3 – Identification and analytical methods, in Micro and Nano Technologies, A. B. T.-H. M. and N. C. for the C. of O. R. Maleki, Ur. Elsevier, (**2022**), 33–51, doi:10.1016/B978-0-12-824527-9.00001-0

[47] F. Zupanič, Gradiva: praktikum, 1st ed. University of Maribor, Faculty of mechanical engineering, (**1999**), ISBN 86-435-0260-X

[48] M. Conserva, G. Donzelli, R. Trippodo, Aluminium and Its Applications. Edimet, University of Pennsylvania State-Edimet: Edimet, PA, USA, (**1992**), 408, ISBN 9788886259019

[49] J. R. Davis, Alloying: understanding the basics, ASM international, Tokyo, Japan, (2001), ISBN 1615030638.

[50] Y. Liao, H. Yan, W. Xia, J. Chen, B. Su, X. Li, L. Zhao, Effect of Heat Treatment on the Microstructure and Properties of High Strain Rate Rolled 7050 Aluminum Alloy, Met. Mater. Int., 28 (**2022**) SE–1, 4, p 1014–1025, doi:10.1007/s12540-020-00961-w

[51] J. Grasserbauer, I. Weißensteiner, G. Falkinger, T. M. Kremmer, P. J. Uggowitzer, S. Pogatscher, Influence of Fe and Mn on the Microstructure Formation in 5xxx Alloys – Part I: Evolution of Primary and Secondary Phases, Materials, 14 (**2021**) 12, doi:10.3390/ma14123204

[52] K. R. Cardoso, D. N. Travessa, W. J. Botta, A. M. Jorge, High Strength AA7050 Al alloy processed by ECAP: Microstructure and mechanical properties, Mater. Sci. Eng. A. Struct. Mater., 528 SE- (**2011**) 18, p 5804–5811, doi:10.1016/j.msea.2011.04.007

[53] H. Wang, Y. Yi, S. Huang, Influence of pre-deformation and subsequent ageing on the hardening behavior and microstructure of 2219 aluminum alloy forgings, J. Alloys Compd., let. 685 SE- (**2016**), p 941–948, doi:10.1016/j.jallcom.2016.06.111

[54] H. Zhu, L. Huang, J. Li, X. Li, H. Ma, C. Wang, F. Ma, Strengthening mechanism in laser-welded 2219 aluminium alloy under the cooperative effects of aging treatment and pulsed electromagnetic loadings, Mater. Sci. Eng. A. Struct. Mater., 714 (**2018**) SE-, 124–139, doi:10.1016/j.msea.2017.12.081

[55] I. S. Zuiko, R. O. Kaibyshev, Towards high strength and ductility of Al–Cu-Mg alloy via cyclic and monotonic pre-straining followed by ageing, J. Alloys Compd., 976 (**2024**), doi:10.1016/j.jallcom.2023.173200

[56] EN ISO 18273:2015 (E) Welding consumables –Wire electrodes, wires and rods for welding of aluminium and aluminium alloys – Classification, CEN-CENELEC Management Centre, Brussels

[57] G. Doria, Choosing a filler metal, Trailer / Body Build., 55 (2014) 8, ISSN: 0041-0772

[58] J. R. Davis, Aluminum and Aluminum Alloys, in Alloying – Understanding the Basics, ASM International, (2001), 2, ISBN: 9780871707444, 0871707446

[59] H. Pinto, A. Pyzalla, H. Hackl, J. Bruckner, A comparative study of microstructure and residual stresses of CMT-, MIG- and laser-hybrid welds, in RESIDUAL STRESSES VII, j. 524–525, nr. 7th European Conference on Residual Stresses (ECRS 7), W. Reimers in S. Quander, Ur. Vienna Univ Technol, Inst Mat Sci & Technol, A-1040 Vienna, Austria, (**2006**), 627–632, doi:10.4028/www.scientific.net/MSF.524-525.627

[60] T. Raza, J. Andersson, L.-E. Svensson, Varestraint Testing of Selective Laser Additive Manufactured Alloy 718—Influence of Grain Orientation, Metals, 9, (**2019**) 10, doi:10.3390/met9101113

[61] X. Zhan, Y. Zhao, Z. Liu, Q. Gao, H. Bu, Microstructure and porosity characteristics of 5A06 aluminum alloy joints using laser-MIG hybrid welding, J. Manuf. Process., 35 (**2018**), 437–445, doi:10.1016/j.jmapro.2018.08.011

[62] I. Bunaziv, O. M. Akselsen, X. Ren, B. Nyhus, M. Eriksson, Laser Beam and Laser-Arc Hybrid Welding of Aluminium Alloys, Metals, 11 (**2021**) 8, doi:10.3390/met11081150

[63] F. Kong, J. Ma, R. Kovacevic, Numerical and experimental study of thermally induced residual stress in the hybrid laser–GMA welding process, J. Mater. Process. Technol., 211, (**2011**) 6, 1102–1111, doi:10.1016/j.jmatprotec.2011.01.012

[64] C. Froustey, J. L. Lataillade, Influence of large pre-straining of aluminium alloys on their residual fatigue resistance, Int. J. Fatigue, 30 (**2008**) 5, 908–916, doi:10.1016/j.ijfatigue.2007.06.011